



# Electrochemical and structural properties of 1,3-substituted (–Cl, –Br) phenyl-5-phenylformazans

Habibe Tezcan \*, Elif Uzluk, Mehmet Levent Aksu

Department of Chemistry, Faculty of Gazi Education, Gazi University, Teknikokullar, 06500 Ankara, Turkey

## ARTICLE INFO

### Article history:

Received 24 November 2007

Received in revised form 11 March 2008

Accepted 25 March 2008

Available online 8 April 2008

### Keywords:

Formazans

Synthesis

Spectroscopy

Substituent effect

Cyclic voltammetry

Ultramicrodisc electrode

Chronoamperometry

## ABSTRACT

In this study, 1-[*o*-, *m*-, *p*-(chloro, bromo)]-3-(*m*-nitrophenyl)-5-phenylformazans were synthesized. Their structures were elucidated and spectral behaviors were investigated using elemental analysis, GC–mass,  $^1\text{H}$  NMR,  $^{13}\text{C}$  NMR, FTIR and UV–vis spectra. Electrochemical properties of formazans such as number of electrons transferred ( $n$ ), diffusion coefficient ( $D$ ) and heterogeneous rate constant ( $k_s$ ) of the compounds were determined and possible mechanisms were proposed with the use cyclic voltammetry, ultramicrodisc electrode and chronoamperometry. The relation between their absorption properties and electrochemical properties was sought. The redox characteristics of these compounds have been investigated in nonaqueous dimethylsulfoxide at platinum and ultramicro platinum (10  $\mu\text{m}$ ) electrodes. Through controlled potential electrolysis, the oxidation products of each class of compounds can be separated and identified. The oxidation mechanism is suggested and it is proved. A correlation was obtained between  $\lambda_{\text{max}}$  with Hammett substituent coefficient,  $E_{\text{ox1}}$  and  $E_{\text{red1}}$ .

© 2008 Elsevier B.V. All rights reserved.

## 1. Introduction

Formazans derivatives with electron donating and withdrawing groups attached to 1,3,5-phenyl ring were synthesized and the effects of substituents on the absorption  $\lambda_{\text{max}}$  values were examined [1–3]. Their bond length, polarity and crystal structures were also determined [4].

Formazans form tetrazolium salt when they are oxidized [5]. Tetrazolium salts are reduced back to formazans by the enzymes in the cell and stain the tissue. Tetrazolium–formazan system is classified as a marker of vitality and this feature enabled the determination of activity on tumor cell [6,7]. This feature caused an increasing interest in the chemistry and especially electrochemistry of formazans.

It was reported that formazans are oxidized in a single 2 electron transfer followed by a deprotonation reaction forming corresponding tetrazolium cation [8]. In a study of the reduction of tetrazolium salts into formazans with superoxide ions, which is supposed to be the cause of aging and various diseases in human body, there were one electron transfer at  $-0.20\text{ V}$  (Ag/AgCl) and one  $1\text{e}^-/\text{H}^+$  transfer at  $-0.40\text{ V}$  (Ag/AgCl) [9].

In this study, seven different novel formazans with various substituents on 1- and 3-phenyl rings have been synthesized. Their structures were elucidated and their spectral behaviors were

investigated using elemental analysis, GC–mass,  $^1\text{H}$  NMR,  $^{13}\text{C}$  NMR, IR and UV–vis spectra. The effect of substituents on  $\lambda_{\text{max}}$  values was determined.

The biological activity of formazan makes the knowledge of its oxidation potentials and possible mechanisms are very important. This study is related to the determination of peak potentials ( $E_{\text{ox}}$ ,  $E_{\text{red}}$ ), diffusion coefficients ( $D$ ), number of electrons transferred ( $n$ ) and standard heterogeneous rate constants ( $k_s$ ) with the use of cyclic voltammetry, ultramicrodisc electrode and chronoamperometry. Separation and identification of the intermediates and the final products were made through controlled potential electrolysis (CPE). A mechanistic scheme for the oxidation of formazan to tetrazolium salt was proposed based upon these data (Scheme 2).

## 2. Experimental

### 2.1. Chemicals

All chemicals were obtained from Merck and Fluka except sodium hydroxide that was purchased from Sigma–Aldrich. All chemicals and solvents used in the syntheses were of reagent grade and were used without further purification. Deionized water (Millipore, Milli-Q) was used for synthesis; the organic solvents:  $\text{CH}_3\text{OH}$ ,  $\text{CH}_3\text{COCH}_3$ , DMSO (dimethylsulfoxide, 99.9%) and 1,4-dioxane were used for electrochemical and spectroscopic measurements. Dimethylsulfoxide was used as solvent. During the solvent purification, all the processes were performed under a dry

\* Corresponding author. Fax: +90 312 2227037.

E-mail address: [habibe@gazi.edu.tr](mailto:habibe@gazi.edu.tr) (H. Tezcan).

oxygen-free argon atmosphere. Fractionation was carried out using a 120 cm column filled with glass spirals at a recoil ratio 50:1. Purified solvent was stored under argon in the dark. DMSO (Merck) was boiled four times with calcium hydride (Merck) for 14 h (5 g/L) and subsequently fractionated at 14 Torr. Finally, the main fraction was carefully fractionated.

## 2.2. Synthesis of 1,3,5-triphenylformazan (1)

A schematic diagram of synthesis route is presented in Scheme 1. 1,3,5-Triphenylformazan (1) was synthesized by the reaction of benzaldehyde (1.06 g, 0.01 mol), phenylhydrazine (1.08 g, 0.01 mol), aniline (0.93 g, 0.01 mol) concentrated HCl (5 ml) and sodium nitrite (0.75 g) in methanol, at 0–5 °C as described in literature [2,3]. Cherry red colored crystals; m.p. 172–173 °C; yield 78%. IR: 3069  $\text{cm}^{-1}$  (aromatic C–H), 3050–3000  $\text{cm}^{-1}$  (N–H), 1600  $\text{cm}^{-1}$  (aromatic C=C), 1500  $\text{cm}^{-1}$  (C=N), 1450  $\text{cm}^{-1}$  (N=N).  $^1\text{H}$  NMR: 8.32–7.27 ppm (15H, aromatic H), 1.18 ppm (1H, azo H).  $^{13}\text{C}$  NMR: 148.80 ppm [1C, (Imino-C) C=N], 141.98–119.54 ppm (8C, other carbons). Elemental Anal. Calc. for  $\text{C}_{19}\text{H}_{16}\text{N}_4$ : C, 76.00; H, 5.33; N, 18.66. Found: C, 75.97; H, 5.29; N, 18.69%. Calc. M: 300.00; Found mass:  $m/z$  (eV) 301.10, 273.10, 223.00, 195.10, 105.05.

### 2.2.1. General procedure for the synthesis of 1-(*o*-, *m*-, *p*-chlorophenyl)-3-(*m*-nitrophenyl)-5-phenylformazans (2–4)

2–4 were synthesized by the reaction of *m*-nitrobenzaldehyde (1.51 g, 0.01 mol), phenylhydrazine (1.08 g, 0.01 mol), *o*-, *m*-, *p*-chloroaniline (1.07 g, 0.01 mol), concentrated HCl (5 ml) and sodium nitrite (0.75 g) in a methanol, at 0–5 °C a method similar to that for 1,3,5-triphenylformazan. Each compound was recrystallized from methanol.

**Selected data for 2.** Red colored crystals; m.p. 175.5–176.5 °C; yield 65%;  $\nu/\text{cm}^{-1}$  3500–3410 (aromatic C–H), 3100–2900 (N–H), 1600 (aromatic C=C), 1530 (C=N), 1350 ( $\text{NO}_2$ ), 1250 (N=N);  $\delta_{\text{H}}$ : 9.03–7.14 (13H, aromatic H), 1.60 (1H, azo H);  $\delta_{\text{C}}$ : 150.82 [(Imino-C) C=N].

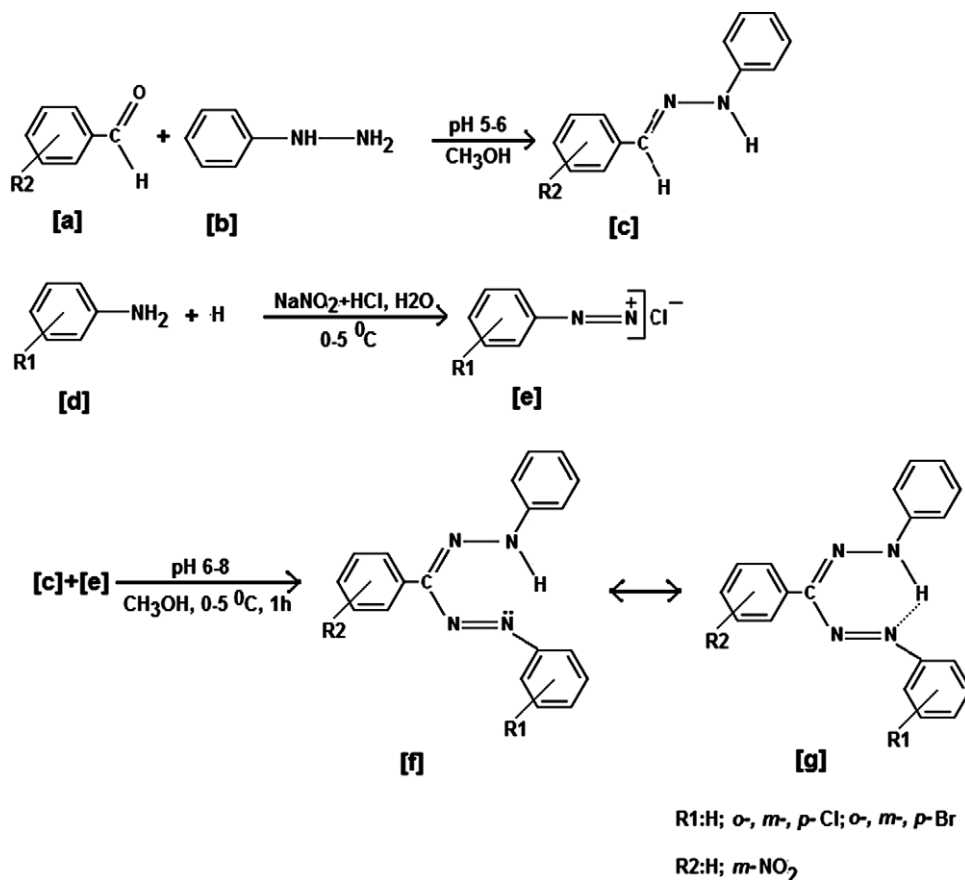
**Selected data for 3.** Dark pink-red colored crystals; m.p. 181.5–183 °C; yield 74%;  $\nu/\text{cm}^{-1}$  3500–3400 (aromatic C–H), 3100–3080 (N–H), 1600 (aromatic C=C), 1530 (C=N), 1350 ( $\text{NO}_2$ ), 1250 (N=N);  $\delta_{\text{H}}$ : 8.96–7.27 (13H, aromatic H), 1.65 (1H, azo H);  $\delta_{\text{C}}$ : 149.62 [(Imino-C) C=N].

**Selected data for 4.** Dark pink-red colored crystals; m.p. 177.5–179 °C; yield 72%;  $\nu/\text{cm}^{-1}$  3480–3400 (aromatic C–H), 3120–3080 (N–H), 1600 (aromatic C=C), 1535 (C=N), 1350 ( $\text{NO}_2$ ), 1250 (N=N);  $\delta_{\text{H}}$ : 8.92–7.21 (13H, aromatic H), 1.59 (1H, azo H);  $\delta_{\text{C}}$ : 149.65 [(Imino-C) C=N]; elemental analysis for  $\text{C}_{19}\text{H}_{14}\text{N}_5\text{O}_2\text{Cl}$  (2–4), M: 379.50, Calc. (%): C, 60.08; H, 3.69; N, 18.44. Found: C, 60.13; H, 3.73; N, 18.50%. Found mass:  $m/z$  (eV): 380.10, 274.00, 139.00, 126.00.

### 2.2.2. General procedure for the synthesis of 1-(*o*-, *m*-, *p*-bromophenyl)-3-(*m*-nitrophenyl)-5-phenylformazans (5–7)

5–7 were synthesized by the reaction of *m*-nitrobenzaldehyde (1.06 g, 0.01 mol), phenyl hydrazine (1.08 g, 0.01 mol), *o*-, *m*-, *p*-bromoaniline (1.75 g, 0.01 mol), concentrated HCl (5 ml) and sodium nitrite (0.75 g) in methanol (50 ml), at 0–5 °C a method similar to that for 1,3,5-triphenylformazan. But each compound was recrystallised from 1,4-dioxane.

**Selected data for 5.** Dark orange-red colored crystals; m.p. 135–136.5 °C; yield 68%;  $\nu/\text{cm}^{-1}$  3490–3410 (aromatic C–H), 3100–3070 (N–H), 1610 (aromatic C=C), 1520 (C=N), 1340 ( $\text{NO}_2$ ), 1250 (N=N);  $\delta_{\text{H}}$ : 9.01–7.08 (13H, aromatic H), 1.60 (1H, azo H);  $\delta_{\text{C}}$ : 150.41 [(Imino-C) C=N].



Scheme 1. Scheme of synthesis route of compounds 1–7.

**Selected data for 6.** Dark red colored crystals; m.p. 145–146 °C; yield 73%;  $\nu/\text{cm}^{-1}$  3490–3410 (aromatic C–H), 2950–2850 (N–H), 1610 (aromatic C=C), 1520 (C=N), 1350 (NO<sub>2</sub>), 1220 (N=N);  $\delta_{\text{H}}$ : 8.94–7.28 (13H, aromatic H), 2.68 (1H, azo H);  $\delta_{\text{C}}$ : 149.62 [(Imino-C) C=N].

**Selected data for 7.** Orange red colored crystals; m.p. 176.5–177.5 °C; yield 70%;  $\nu/\text{cm}^{-1}$  3490–3410 (aromatic C–H), 2950–2850 (N–H), 1610 (aromatic C=C), 1540 (C=N), 1350 (NO<sub>2</sub>), 1220 (N=N);  $\delta_{\text{H}}$ : 8.85–6.93 (13H, aromatic H), 2.24 (1H, azo H);  $\delta_{\text{C}}$ : 149.61 [(Imino-C) C=N]; elemental analysis for C<sub>19</sub>H<sub>14</sub>N<sub>5</sub>O<sub>2</sub>Br (**5–7**), M: 423.90, Calc.: C, 53.78; H, 3.30; N, 16.51. Found: C, 53.70; H, 3.27; N, 16.55%. Found mass:  $m/z$  (eV): 425.00, 318.30, 240.00, and 170.10.

**1–7** were purified by repeated crystallization, dried under reduced pressure and the purity was checked by thin layer chromatography.

### 2.3. Oxidation product of 1

Elemental analysis calculated: C, 76.25; H, 5.02; N, 18.73. Found: C, 76.40; H, 5.18; N, 18.70%. Mass:  $m/z$  (eV), Calculated M.: 299.00. Mass spectrum: shows the main fragments at  $m/z$  299.10, parent 222.10; 194.30; 105.00.

### 2.4. Oxidation product of 3

Elemental analysis calculated: C, 60.24; H, 3.43; N, 18.49. Found: C, 60.30; H, 3.55; N, 18.35%. Mass:  $m/z$  (eV), Calculated M.: 378.50. Mass spectrum: shows the main fragments at  $m/z$  378.60, parent 343.00; 239.00; 139.50.

### 2.5. Oxidation product of 6

Elemental analysis calculated: C, 53.91; H, 3.07; N, 16.55. Found: C, 54.00; H, 3.15; N, 16.43%. Mass:  $m/z$  (eV), Calculated M.: 422.90. Mass spectrum: shows the main fragments at  $m/z$  423.00, parent 343.20; 239.10; 183.90.

### 2.6. Electrochemical measurements

Electrochemical studies were carried out with a computerized CHI Instrument 660 B system in a conventional three-electrode cell. A platinum electrode (PE) (CHI102) and a 10  $\mu\text{m}$ -platinum ultramicrodisc electrode (UME) (CHI107) were used as working electrode. The electrodes were cleaned by electrochemical potential cycling and washed with excess dimethyl sulfoxide. A platinum wire was used as the auxiliary electrode. The reference electrode was a silver wire in constant contact with 0.1 M AgNO<sub>3</sub> in dimethylsulfoxide. Ferrocene (Fc) was used as an internal standard to measure formal potential  $E^0$  vs. Fc<sup>0</sup>/Fc<sup>+</sup>. All measurements were carried out with  $1 \times 10^{-4}$  mol of the reactant in 10 mL dry oxygen-free solvent with 0.1 mol dm<sup>-3</sup> tetrabutylammonium tetrafluoroborate (TBA<sup>+</sup>BF<sub>4</sub><sup>-</sup>) as supporting electrolyte. All solutions were deaerated for 10 min with pure argon. All the measurements were taken at room temperature, 25 °C. The voltage scan rate range during the CV measurements was 10–10,000 mV s<sup>-1</sup>.

### 2.7. Spectroscopic measurements

The UV–vis spectra of the formazans synthesized in this study were obtained with UNICAM UV2-100 UV–visible spectrophotometer using 1 cm quartz cells in  $10^{-5}$  mol l<sup>-1</sup> DMSO using a 325 nm lamp in the range of 250–600 nm. IR spectra were recorded on a MATT-SON 100-FT-IR spectrophotometer between 4000 and 400 cm<sup>-1</sup> using KBr pellets. <sup>1</sup>H NMR spectra were performed on a Bruker AVANCE DPX-400 MHz and <sup>13</sup>C NMR 100 MHz spectro-

photometer using CDCl<sub>3</sub> and *d*<sub>6</sub>-DMSO,  $10^{-4}$  mol l<sup>-1</sup>. Elemental analyses were carried out using a LECO-CHNS-932 elemental analyzer. Mass spectra were recorded using on an AGILENT 1100 MSD mass spectrometer.

## 3. Result and discussion

### 3.1. Electrochemical properties

#### 3.1.1. Cyclic voltammetry results

The electrochemical properties of formazans in DMSO were investigated using voltammetric techniques. The cyclic voltammograms of formazans substituted with –Cl and –Br at the *o*-, *m*-, *p*-positions of the 1-phenyl ring and –NO<sub>2</sub> at the *m*-position of the 3-phenyl ring (**2–7**) are compared with the parent compound TPF (**1**). Figs. 1–3 show cyclic voltammograms of these compounds. All the cyclic voltammetric data are tabulated in Tables 1 and 2.

A cyclic voltammogram of TPF (**1**) is shown in Fig. 1. The scan showed two anodic waves and two cathodic waves. There were two major oxidation peaks in the cyclic voltammogram of TPF (**1**) corresponding to the formation of formazan radical (TPF<sup>•</sup>) at –1390.3 mV and tetrazolium cation (TPT<sup>+</sup>) at –688.9 mV. Also two cathodic peaks ( $E_{\text{red1}}$ ,  $E_{\text{red2}}$ ) are observed at –426.0 mV and –815.1 mV for TPF (**1**) (Fig. 1). When employed the scan rates were 10, 100, 1000, 10,000 mV s<sup>-1</sup>, anodic peak potentials  $E_{\text{ox1}}$  were obtained –1467.9 mV, –1390.3 mV, –1311.4 mV, –1298.0 mV, respectively (Table 2). When the scan rate was increased, anodic peak potentials  $E_{\text{ox1}}$  shifted towards anodic value in accordance with the quasi-reversible process.

It seem that the substituted groups (–Cl and –Br) have quite effect upon the electrochemical behavior of formazans in Figs. 2 and 3. As seen from Fig. 2 and Table 1, the substitution of the 1-phenyl ring with chloro at the *o*-, *m*-, *p*-positions (**2–4**) caused changes in both the anodic and cathodic peak potential and the peak currents as compared with the parent TPF (**1**).

At the oxidation of –Cl substituted formazans, oxidation peaks were observed more anodic potential in the *o*-, *m*-, *p*-Cl (**2–4**) compared with TPF (**1**). The scan of **2** showed one anodic wave and two cathodic waves. A cyclic sweep in the –1.60 to +0.00 V range is shown one anodic peak at  $E_{\text{ox1}} = -1246.0$  mV and two cathodic peaks at  $E_{\text{red1}} = -609.7$  mV,  $E_{\text{red2}} = -1049.0$  (Fig. 2a). When employed the scan rates were 10, 100, 1000, 10,000 mV s<sup>-1</sup>, anodic peak potentials  $E_{\text{ox1}}$  were obtained –1283.3 mV, –1246.0 mV,

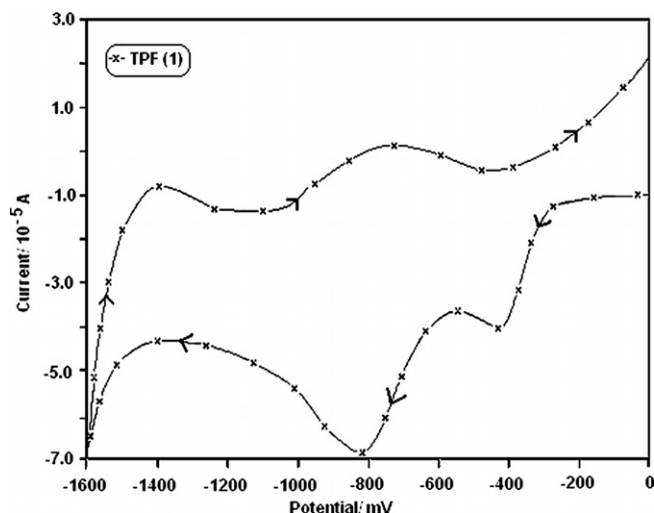


Fig. 1. Cyclic voltammogram of a DMSO solution of  $1.0 \times 10^{-4}$  M TPF (**1**) in the presence of 0.1 M TBA<sup>+</sup>BF<sub>4</sub><sup>-</sup> at Pt electrode. Potential scan rate: 100 mV s<sup>-1</sup>.

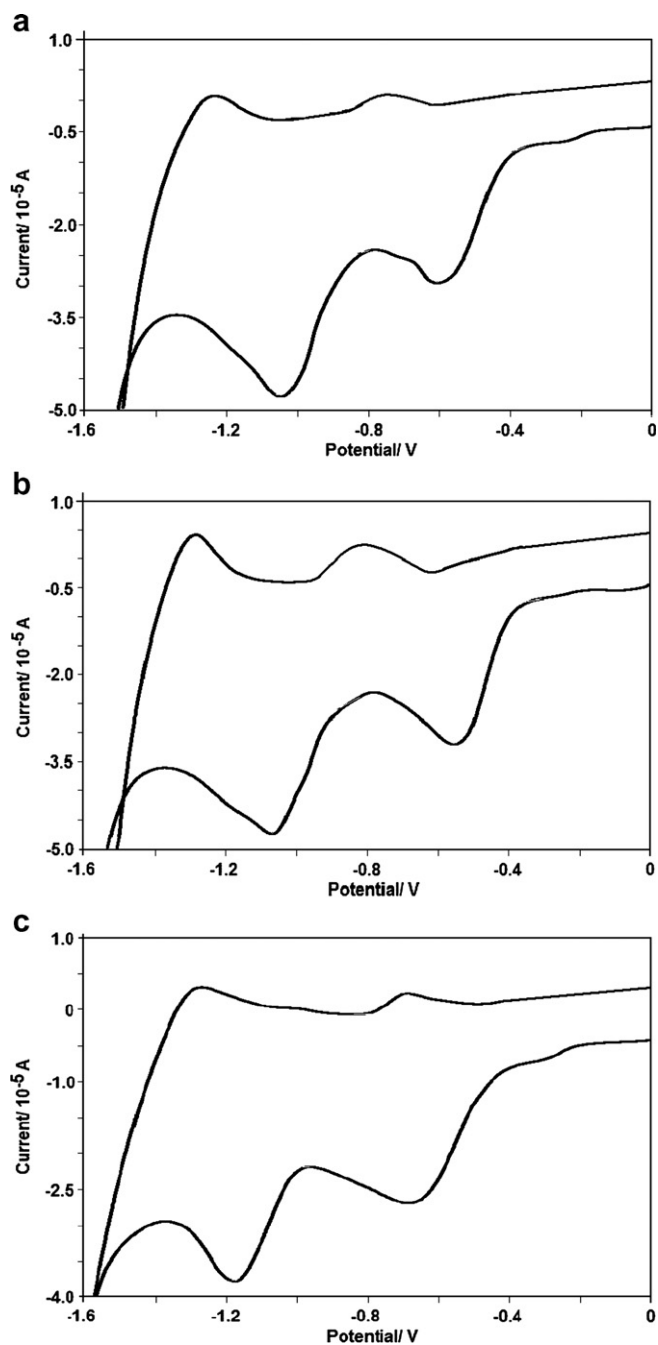


Fig. 2. Representative cyclic voltammogram in DMSO (25 °C, ionic strength: 0.1 M TBA<sup>+</sup>BF<sub>4</sub><sup>-</sup>,  $v$ : 100 mV s<sup>-1</sup>): (a) compound 2; (b) 3; (c) 4.

–1044.9 mV, –626.4 mV, respectively (Table 2). When the scan rate was increased, anodic peak potentials  $E_{ox1}$  shifted towards anodic value in accordance with the quasi-reversible process. The CV behaviour of compound (2) is similar to that of TPF (1). In this case, however, the anodic peak of the “product” is shifted to about 145 mV higher potentials as compared to the CV curve of TPF (1).

The scan of 3 showed two anodic waves and two cathodic waves. A cyclic sweep in the –1.60 to +0.00 V range is shown two anodic peaks at  $E_{ox1} = -1284.3$  mV,  $E_{ox2} = 805.9$  and two cathodic peaks at  $E_{red1} = -552.1$  mV,  $E_{red2} = -1067.0$  (Fig. 2b). When employed the scan rates were 10, 100, 1000, 10,000 mV s<sup>-1</sup>, anodic peak potentials  $E_{ox1}$  were obtained –1312.6 mV, –1284.3 mV, –1099.7 mV, –726.7 mV, respectively (Table 2). When the scan rate was increased, anodic peak potentials  $E_{ox1}$

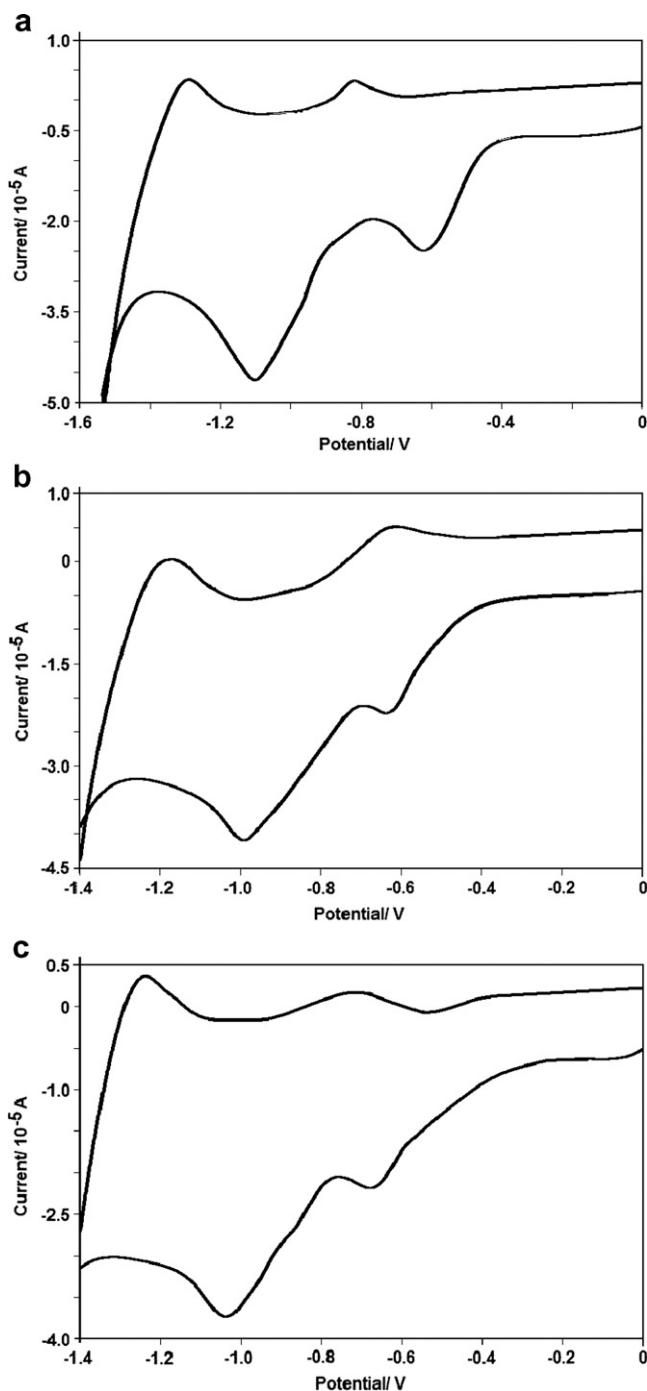


Fig. 3. Representative cyclic voltammogram in DMSO (25 °C, ionic strength: 0.1 M TBA<sup>+</sup>BF<sub>4</sub><sup>-</sup>,  $v$ : 100 mV s<sup>-1</sup>): (a) compound 5; (b) 6; (c) 7.

shifted towards anodic value in accordance with the quasi-reversible process.

In the –1.60 to +0.00 V range, two anodic peaks ( $E_{ox1}$ ,  $E_{ox2}$ ) are appeared at –1268.5 mV, –680.3 mV, respectively 4. Two cathodic peaks ( $E_{red1}$ ,  $E_{red2}$ ) are observed at –682.9 mV, –1174.4 mV (Fig. 2c). These results also are in accordance with the spectroscopic data. When employed the scan rates were 10, 100, 1000, 10,000 mV s<sup>-1</sup>, anodic peak potentials  $E_{ox1}$  were obtained –1298.8 mV, –1268.5 mV, –994.6 mV, –963.1 mV, respectively (Table 2). When the scan rate was increased, anodic peak potentials  $E_{ox1}$  shifted towards anodic value in accordance with the quasi-reversible process.

**Table 1**  
Voltamperometric results of formazans (1–7)

Compound	$E_{ox1}$ (mV)	$I_{pox1}$ (A)	$E_{ox2}$ (mV)	$I_{pox2}$ (A)	$E_{red1}$ (mV)	$I_{pred1}$ (A)	$E_{red2}$ (mV)	$I_{pred2}$ (A)	$\Delta E_p$	$k_s$ (cm s <sup>-1</sup> )
1	-1390.3	$3.086 \times 10^{-6}$	-740.7	$1.789 \times 10^{-6}$	-426.0	$2.657 \times 10^{-6}$	-815.1	$6.098 \times 10^{-6}$	-565.2	$7.722 \times 10^{-3}$
2	-1246.0	$6.300 \times 10^{-7}$	-	-	-609.7	$2.953 \times 10^{-5}$	-1049.0	$4.781 \times 10^{-5}$	-636.3	$5.877 \times 10^{-3}$
3	-1284.3	$4.165 \times 10^{-6}$	-805.9	$1.499 \times 10^{-6}$	-552.1	$3.199 \times 10^{-5}$	-1067.0	$4.733 \times 10^{-5}$	-732.2	$9.585 \times 10^{-3}$
4	-1268.5	$3.017 \times 10^{-6}$	-680.3	$2.149 \times 10^{-6}$	-682.9	$2.673 \times 10^{-5}$	-1174.4	$3.767 \times 10^{-5}$	-585.6	$5.714 \times 10^{-3}$
5	-1289.4	$3.504 \times 10^{-6}$	-818.8	$3.163 \times 10^{-6}$	-622.7	$2.484 \times 10^{-5}$	-1098.7	$4.617 \times 10^{-5}$	-666.7	$5.246 \times 10^{-3}$
6	-1171.7	$2.107 \times 10^{-7}$	-602.0	$5.167 \times 10^{-6}$	-638.8	$2.211 \times 10^{-5}$	-991.0	$4.109 \times 10^{-5}$	-532.9	$10.628 \times 10^{-3}$
7	-1235.7	$3.605 \times 10^{-6}$	-714.2	$1.561 \times 10^{-6}$	-677.6	$2.191 \times 10^{-5}$	-1036.0	$3.738 \times 10^{-5}$	-558.1	$2.780 \times 10^{-3}$

Column 10:  $\Delta E_p$ :  $E_{ox1} - E_{red1}$  (mV). Cyclic voltammograms were obtained in DMSO at 25 °C at platinum electrode, ionic strength 0.1 M (TBA<sup>+</sup>BF<sub>4</sub><sup>-</sup>), sweep speed: 100 mV s<sup>-1</sup>.  $E_{ox}$ : oxidation;  $E_{red}$ : reduction,  $k_s$ /cm s<sup>-1</sup> values.

**Table 2**  
Voltamperometric data of formazans (1–7) in DMSO at platinum electrode and 25 °C, ionic strength 0.1 M (TBA<sup>+</sup>BF<sub>4</sub><sup>-</sup>), scan rates: 10, 1000 and 10,000 mV s<sup>-1</sup>

Compound	Scan rate (mV s <sup>-1</sup> )	$E_{ox1}$ (mV)	$I_{pox1}$ (A)	$E_{ox2}$ (mV)	$I_{pox2}$ (A)	$E_{red1}$ (mV)	$I_{pred1}$ (A)	$E_{red2}$ (mV)	$I_{pred2}$ (A)
1	10	-1467.9	$2.133 \times 10^{-7}$	-	-	-1047.0	$2.625 \times 10^{-5}$	-	-
	1000	-1311.4	$1.111 \times 10^{-4}$	-	-	-237.4	$3.261 \times 10^{-5}$	-	-
	10,000	-1298.0	$7.896 \times 10^{-6}$	-	-	-	-	-	-
2	10	-1283.3	$2.230 \times 10^{-6}$	-1218.9	$2.893 \times 10^{-6}$	-559.0	$2.283 \times 10^{-6}$	-819.0	$4.832 \times 10^{-6}$
	1000	-1044.9	$1.191 \times 10^{-4}$	-	-	-197.0	$1.072 \times 10^{-4}$	-	-
	10,000	-626.4	$6.145 \times 10^{-4}$	-	-	-409.3	$7.942 \times 10^{-4}$	-	-
3	10	-1312.6	$8.928 \times 10^{-6}$	-	-	-616.0	$1.011 \times 10^{-5}$	-910.7	$1.380 \times 10^{-6}$
	1000	-1099.7	$1.917 \times 10^{-4}$	-	-	-266.0	$2.425 \times 10^{-4}$	-	-
	10,000	-726.7	$6.243 \times 10^{-4}$	-	-	-511.7	$1.167 \times 10^{-3}$	-	-
4	10	-1298.8	$3.959 \times 10^{-6}$	-	-	-765.9	$7.599 \times 10^{-6}$	-1097.4	$1.582 \times 10^{-5}$
	1000	-994.6	$6.371 \times 10^{-5}$	-528.0	$9.214 \times 10^{-6}$	-803.0	$6.459 \times 10^{-6}$	-1280.0	$8.283 \times 10^{-5}$
	10,000	-963.1	$6.390 \times 10^{-5}$	-	-	-460.6	$6.906 \times 10^{-5}$	-942.0	$1.276 \times 10^{-4}$
5	10	-1279.6	$5.298 \times 10^{-6}$	-798.7	$3.204 \times 10^{-6}$	-583.0	$2.535 \times 10^{-6}$	-1132.7	$1.193 \times 10^{-5}$
	1000	-1072.2	$9.843 \times 10^{-5}$	-592.0	$4.050 \times 10^{-6}$	-696.7	$5.261 \times 10^{-5}$	-	-
	10,000	-426.0	$1.641 \times 10^{-5}$	-	-	-335.0	$3.037 \times 10^{-5}$	-	-
6	10	-1165.7	$4.103 \times 10^{-6}$	-701.5	$2.296 \times 10^{-6}$	-637.5	$8.356 \times 10^{-6}$	-967.5	$1.382 \times 10^{-5}$
	1000	-1013.5	$9.843 \times 10^{-5}$	-507.9	$6.415 \times 10^{-5}$	-377.8	$2.955 \times 10^{-5}$	-1080.5	$1.115 \times 10^{-4}$
	10,000	-558.3	$3.698 \times 10^{-4}$	-	-	-260.5	$1.722 \times 10^{-4}$	-1202.3	$3.911 \times 10^{-4}$
7	10	-1288.7	$5.375 \times 10^{-6}$	-	-	-273.8	$8.428 \times 10^{-6}$	-919.9	$1.694 \times 10^{-5}$
	1000	-1050.2	$1.578 \times 10^{-4}$	-	-	-219.0	$1.778 \times 10^{-4}$	-	-
	10,000	-631.0	$6.010 \times 10^{-4}$	-	-	-473.8	$9.767 \times 10^{-4}$	-	-

$E_{ox}$ : oxidation;  $E_{red}$ : reduction.

The intensity of the first peak changes as ( $E_{ox1}$ ) for compound (3) are much higher compared with the compound (2). This shows that the electron transfer rate is low in compound (2). The intensity of the first peak ( $E_{ox1}$ ) is much higher for compound (3) compared with those of 2, 4.

As seen from Fig. 3 and Table 1, compounds 5–7 caused changes in both the anodic and cathodic peak potential and the peak currents as compared with the parent TPF (1). The first oxidation peak ( $E_{ox1}$ ) have shifted as appropriate to the electron donating of the Br (5–7) compared to TPF (1).

The scans of 5–7 showed two anodic waves and two cathodic waves. A cyclic sweep in the -1.60 to +0.00 V range is shown two anodic peaks at  $E_{ox1} = -1289.4$  mV,  $E_{ox2} = 818.8$  and two cathodic peaks at  $E_{red1} = -622.7$  mV,  $E_{red2} = -1098.7$  (Fig. 3a). When employed the scan rates were 100, 1000, 10,000 mV s<sup>-1</sup>, anodic peak potentials  $E_{ox1}$  were obtained -1289.4 mV, -1072.2 mV, -426.0 mV, respectively (Table 2). When the scan rate was increased, anodic peak potentials  $E_{ox1}$  shifted towards anodic value in accordance with the quasi-reversible process. The CV behaviour of compound (5) is similar to that of TPF (1). In this case, however, the anodic peak of the “product” is shifted to about 110 mV higher potentials as compared to the CV curve of TPF (1).

In the -1.60 to +0.00 V range, two anodic peaks ( $E_{ox1}$ ,  $E_{ox2}$ ) are appeared at -1171.7 mV, -602.0 mV, respectively 6 (Fig. 3b). Two cathodic peaks ( $E_{red1}$ ,  $E_{red2}$ ) are observed at -638.8 mV, -991.0 mV (Fig. 3b). When employed the scan rates were 100, 1000,

10,000 mV s<sup>-1</sup>, anodic peak potentials  $E_{ox1}$  were obtained -1171.7 mV, -1013.5 mV, -558.3 mV, respectively (Table 2). When the scan rate was increased, anodic peak potentials  $E_{ox1}$  shifted towards anodic value in accordance with the quasi-reversible process.

In the -1.60 to +0.00 V range, two anodic peaks ( $E_{ox1}$ ,  $E_{ox2}$ ) are appeared at -1235.7 mV, -714.2 mV, respectively for 7 (Fig. 3c). Two cathodic peaks ( $E_{red1}$ ,  $E_{red2}$ ) are observed at -677.6 mV, -1036.0 mV (Fig. 3c). When employed the scan rates were 100, 1000, 10,000 mV s<sup>-1</sup>, anodic peak potentials  $E_{ox1}$  were obtained -1288.7 mV, -1235.7 mV, -1050.2 mV, -631.0 mV, respectively (Table 2). When the scan rate was increased, anodic peak potentials  $E_{ox1}$  shifted towards anodic value in accordance with the quasi-reversible process.

The intensity of the first peak changes as ( $E_{ox1}$ ) for compound (7) are much higher compared with the compound (6). This shows that the electron transfer rate is low in compound (6). The intensity of the first peak ( $E_{ox1}$ ) is much higher for compound (7) compared with those of 5, 6.

The first oxidation peak potentials ( $E_{ox1}$ ) were observed at anodic potential values in substituted -Br formazans (6, 7) shifted to more cathodic potential values in substituted -Cl formazans (2, 4). At *o*-position Cl (2) is inductively electron withdrawing and electron donating as a result of resonance. Since these effects oppose to each other *o*-position has the least electron donating effect to the system and the potential value observed verifies this fact.

For *m*-Cl (**3**), both the inductive and resonance effect decrease so the potential show a higher shift towards the anodic values. At *p*-position (**4**), the inductive effect completely diminishes and resonance effect predominates. Similar arguments are valid for Br substitution. The difference may stem from the difference in electronegativity values. These results also are in accordance with the spectroscopic data.

Consequently, peak potentials are dependent upon the type and position of substituents.

### 3.1.2. Ultramicrodisc and chronoamperometry results

The number of electrons transferred was obtained with the use of chronoamperometry Cottrell equation (1)

$$i_t = \frac{nFACD^{1/2}}{\pi^{1/2}t^{1/2}} \quad (1)$$

and ultramicrodisc electrode (UME) steady-state current (2) [10]

$$i_{ss} = 4rnFCD \quad (2)$$

The real surface area of the Pt electrode was found to be 2.58 cm<sup>2</sup> with the use ferrocene. If  $i_t$  values are plotted against  $t^{-1/2}$  the resulting slope (3) will be

$$\text{Slope} = \left(\frac{nFC}{\pi r}\right)^{1/2} A \quad (3)$$

from which  $n$  could easily be calculated. The  $n$  values calculated are tabulated in Table 3.

As seen from Table 3 and Fig. 4 there are two-step one-electron transfer waves for the parent compound TPF (**1**) that the compound gives first formazan radical (TPF<sup>•</sup>) followed by the formation of tetrazolium cations (TPT<sup>+</sup>). TPF (**1**) is oxidized in two quasi-reversible two-electron process to the corresponding tetrazolium cation (TPT<sup>+</sup>). Mechanism of the oxidation of TPF (**1**) is shown in Scheme 2a. These results are in agreement with the literature [9].

The number of electrons transferred is two for *o*-*m*-, *p*-Cl substituted formazans and *o*-*m*-, *p*-Br substituted formazans in UME-based cyclic voltammograms and chronoamperometry (Table 3).

As seen from Figs. 4b and 5a, there are two one-electron transfer waves for *o*-Cl and *o*-Br the substituted formazans (**2**, **5**). *o*-Br substituted formazan gave clear S-shaped steady-state current ( $i_{ss}$ ) with UME. The number of electrons transferred is two for *o*-Cl substituted formazan and *o*-Br substituted formazan in UME-based cyclic voltammograms and chronoamperometry (Table 3). This is in accordance with CV results (Figs. 2a and 3a). They (**2**, **5**) are oxidized in two quasi-reversible two-electron process to the corresponding tetrazolium cation. Mechanisms of the oxidation of **2**, **5** are shown in Scheme 2a. These results are in agreement with the literature [9].

As seen from Table 3 and Figs. 4c and 5b, there are one-step two electrons transfer waves for the case of *m*-Cl and *m*-Br substituted formazans (**3**, **6**). Compounds (**3**, **6**) are oxidized in a single quasi-reversible two-electron process to the corresponding tetrazolium

cation. Mechanisms of the oxidation of **3**, **6** are shown in Scheme 2b. These results are in agreement with the literature [8].

*p*-Cl and *p*-Br the substituted formazans (**4**, **7**) form the substituted formazan radicals from the substituted formazan anions through one-electron loss which is followed by one-electron loss to give the corresponding tetrazolium cations. The two-electron oxidation products (substituted tetrazolium tetrafluoroborate) are formed through oxidation of the parent substituted formazan to radicals (substituted formazan radicals) and then cyclised. Mechanisms of the oxidation of **4**, **7** are shown in Scheme 2a. These results are in agreement with the literature [9].

### 3.1.3. Diffusion coefficients and the heterogenous rate constants results

The diffusion coefficients **1–7** were determined the use of Baranski UME technique [10]. The values given in Table 3 were in the expected dimensions. The  $k_s$  values were determined with the use of Klinger–Kochi equation [11] as the potential difference for the anodic and cathodic peak currents for the second peak was more than 500 mV. The  $k_s$  values under these circumstances are dependent on the scan rate, diffusion coefficient, oxidation and reduction peak potentials.

$$k_s = 2.18 \left(\frac{D\alpha nFv}{RT}\right)^{1/2} \exp\left[-\frac{\alpha nF}{RT}(E_p^a - E_p^c)\right]$$

$$\alpha = 1857 \left[\frac{RT}{nF(E_p - E_{p/2})}\right]$$

The resulting data are tabulated in Table 1. The oxidation of the formazan derivatives was found to be quasi-reversible due to the facts that  $\Delta E_p$  is larger than 59/ $n$  (mV), which increased with the scan rate, and the shift of the anodic peak potential  $E_{ox}$  towards positive values with increasing scan rate. The case  $2 \times 10^{-5} v^{1/2} < k_s < 0.3 v^{1/2}$  corresponds to a quasi-reversible situation. The  $k_s$  values obtained in this study fall into this range. Change of the  $k_s$  values in the order: *m* → *o* → *p*-substitutions for -Cl-substituted formazans and -Br-substituted formazans. The  $k_s$  value of *m*-Br substituted formazan is comparatively larger than the others.

### 3.2. Spectral properties

Elemental analysis and mass spectroscopic data are corroborated the structures proposed in Scheme 1. When one examines <sup>1</sup>H NMR data the aromatic H and NH peaks for TPF (**1**) appear at  $\delta = 8.37$ – $7.27$  ppm and  $\delta = 1.18$  ppm. Normally, one would expect aromatic H peak on a single benzene ring at  $\delta = 7.27$  ppm. The weak electron withdrawing effect of the other phenyl rings and the double bond resonance in the CNNC skeleton of the formazan caused the aromatic-H peak to shift towards lower fields. This is an expected outcome [12,13]. In **2–7** where position of the 3-phenyl ring is substituted with *m*-NO<sub>2</sub>, while 1-phenyl ring is substituted by -Cl and -Br at the *o*-, *m*-, *p*-positions, the aromatic-H signals are shifted towards lower fields. This is in accordance with the electron withdrawing properties of *m*-NO<sub>2</sub>. On the other hand,

**Table 3**  
Some of the parameters calculated for formazans (**1–7**)

Compound	Abbreviation	C* /mM	$i_{ss}$ /A	Cottrell slope/S	$n$	$n$ net	D /cm <sup>2</sup> s <sup>-1</sup>
<b>1</b>	TPF (peak 1)	7.3	$9.081 \times 10^{-10}$	$1.599 \times 10^{-5}$	0.75	1	$4.297 \times 10^{-6}$
<b>1</b>	TPF (peak 2)	7.3	$1.621 \times 10^{-9}$	$2.109 \times 10^{-5}$	0.73	1	$7.880 \times 10^{-6}$
<b>2</b>	–	5.0	$1.413 \times 10^{-9}$	$2.695 \times 10^{-5}$	1.99	2	$3.679 \times 10^{-6}$
<b>3</b>	–	6.4	$4.104 \times 10^{-9}$	$3.677 \times 10^{-5}$	1.83	2	$8.306 \times 10^{-6}$
<b>4</b>	–	7.0	$1.870 \times 10^{-9}$	$2.596 \times 10^{-5}$	1.78	2	$3.460 \times 10^{-6}$
<b>5</b>	–	7.0	$1.323 \times 10^{-9}$	$2.901 \times 10^{-5}$	1.76	2	$2.782 \times 10^{-6}$
<b>6</b>	–	7.8	$3.284 \times 10^{-9}$	$4.735 \times 10^{-5}$	1.70	2	$5.454 \times 10^{-6}$
<b>7</b>	–	7.3	$1.027 \times 10^{-9}$	$2.514 \times 10^{-5}$	1.64	2	$2.222 \times 10^{-6}$

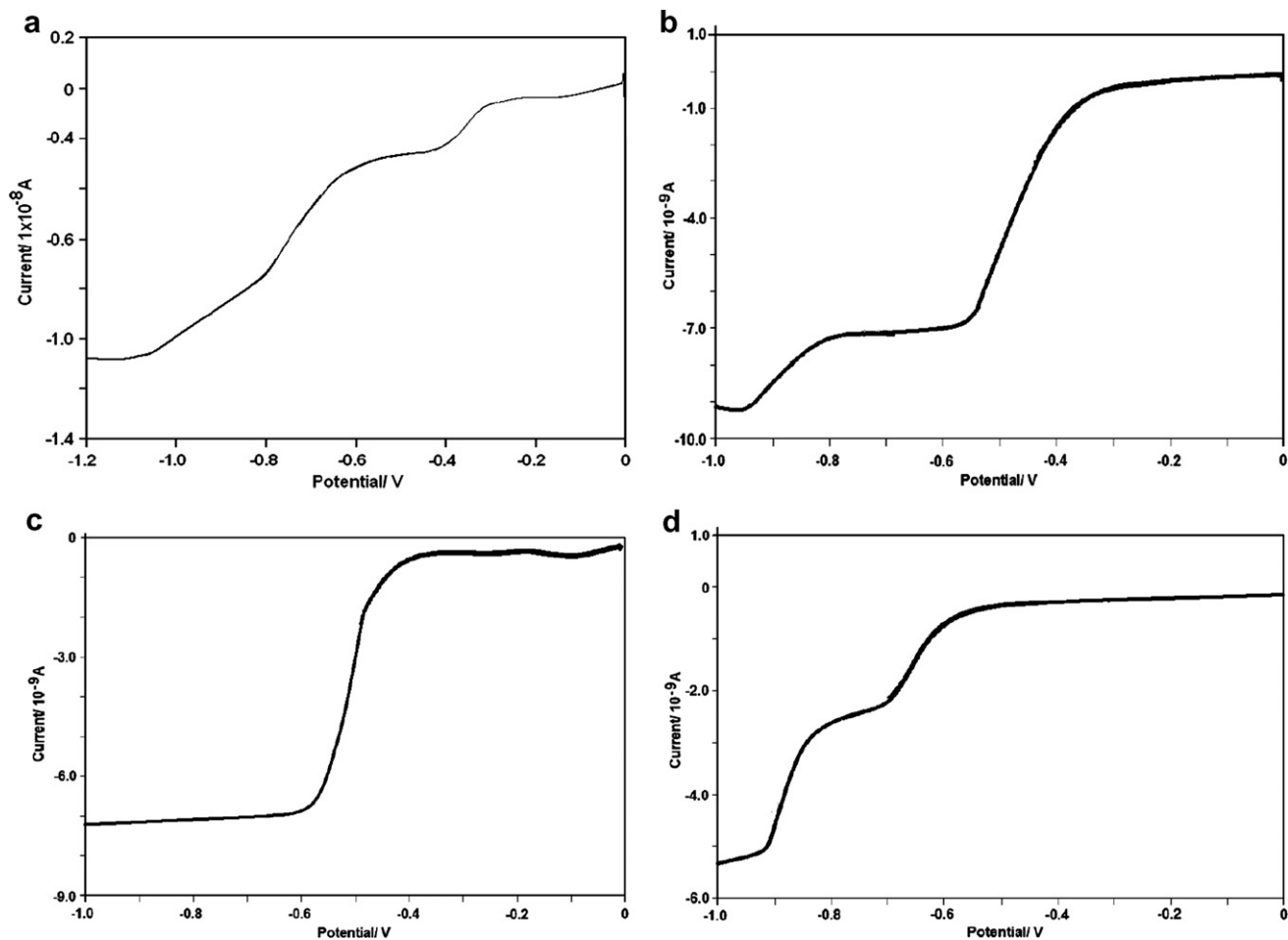
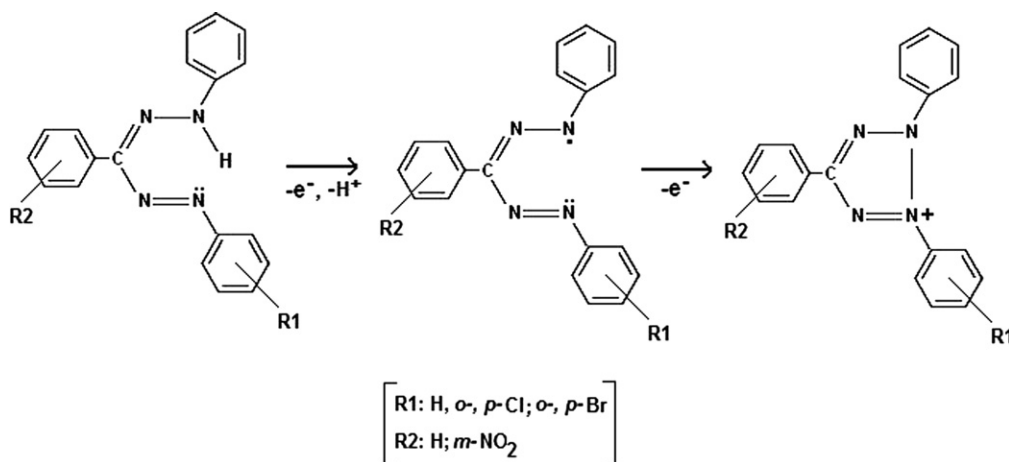


**Fig. 4.** UME curves of DMSO solutions of  $1.0 \times 10^{-4}$  M compounds **1** (a); **2** (b); **3** (c); **4** (d) in the presence of 0.1 M TBA<sup>+</sup>BF<sub>4</sub><sup>-</sup> at 10 μm-platinum ultramicro electrode. Potential scan rate: 10 mV s<sup>-1</sup>.



**Scheme 2a.** Possible oxidation mechanism for **1**, **2**, **4**, **5**, **7**.

Cl and Br are electron withdrawing due to inductive and electron donating due to resonance effects. At the *o*-position the electron withdrawing effect dominates which is added to the electron withdrawing effect of *m*-NO<sub>2</sub> which caused the H peak of TPF (**1**) at 8.37–7.21 ppm shifted towards lower field at 9.03–7.14 ppm. At the *m*-position both the inductive and resonance effects decrease so the shift towards the lower fields is relatively smaller. At the

*p*-position inductive effect almost disappears and resonance effect predominates and Cl acts as an electron donating group resulted the H peak to be shifted slightly to higher fields. Same arguments are also true for the substitution of the 1-phenyl ring at the *o*-, *m*- and *p*-positions. The difference stems from the difference in their electronegativities. When one examines <sup>13</sup>C NMR data one sees a 9C signal in contrast to 13C signal for TPF (**1**). This shows that

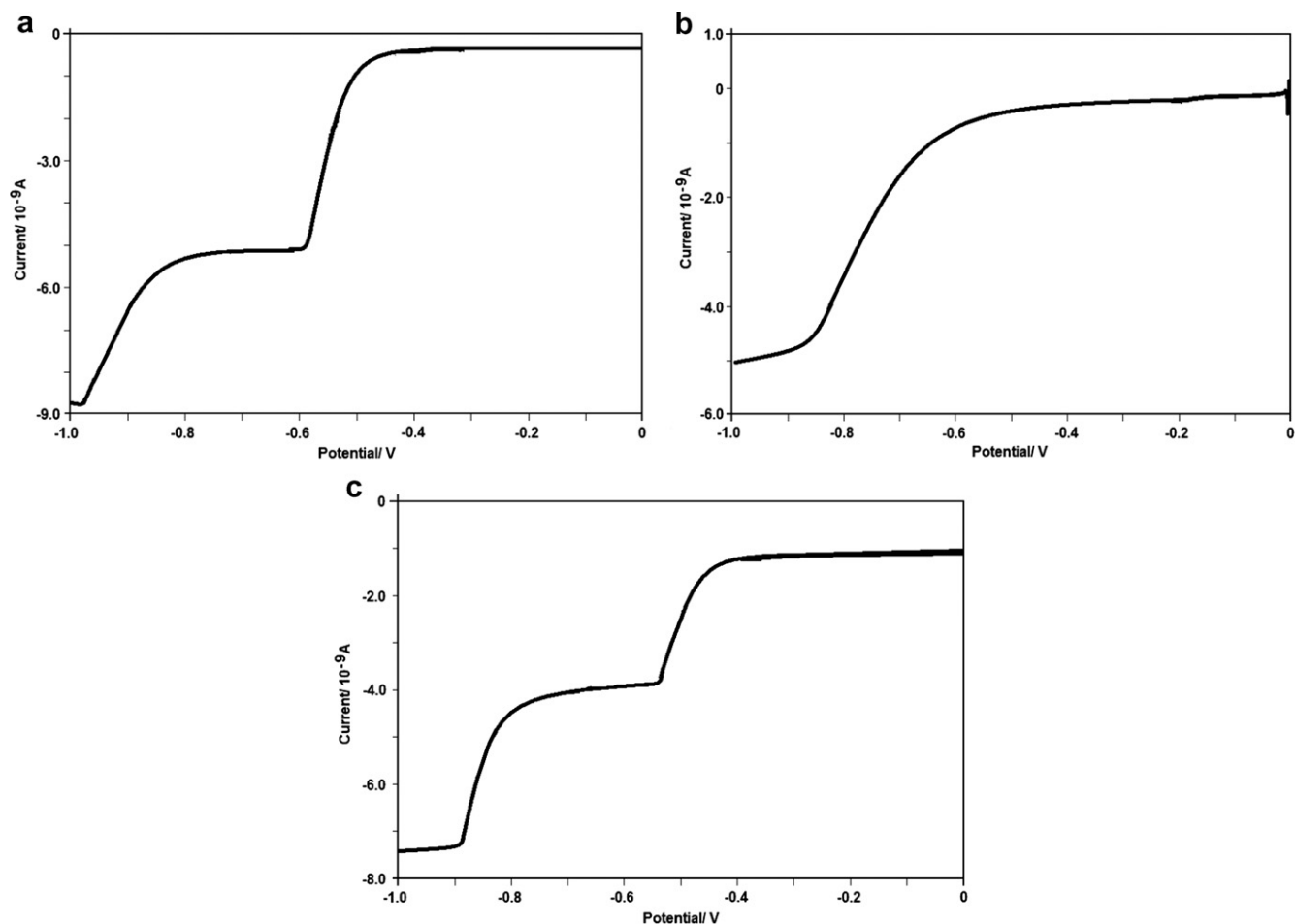
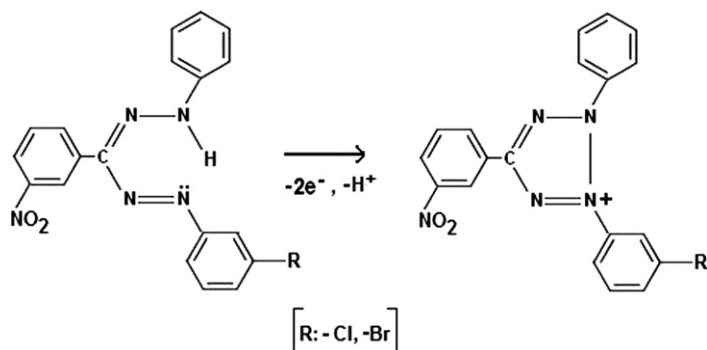


Fig. 5. UME curves of DMSO solutions of  $1.0 \times 10^{-4}$  M compounds **5** (a); **6** (b); **7** (c) in the presence of 0.1 M  $\text{TBA}^+\text{BF}_4^-$  at  $10 \mu\text{m}$ -platinum ultramicro electrode. Potential scan rate:  $10 \text{ mV s}^{-1}$ .

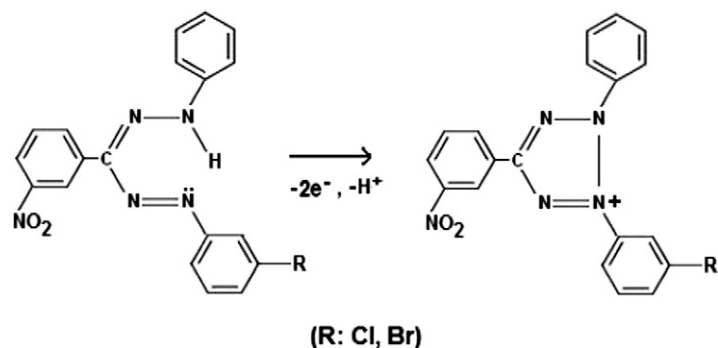
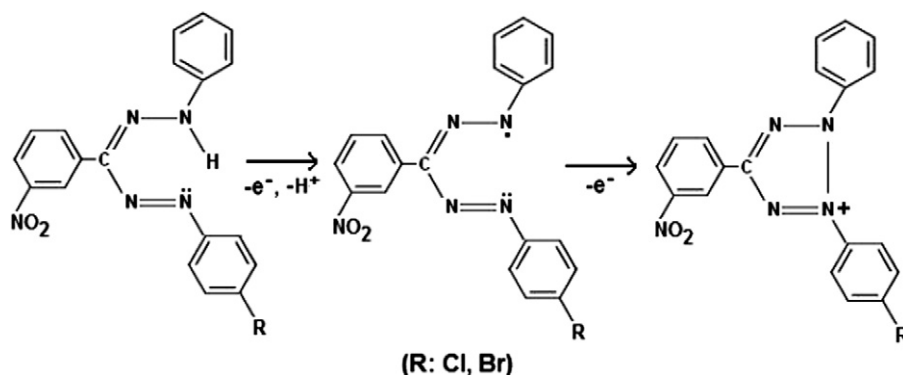
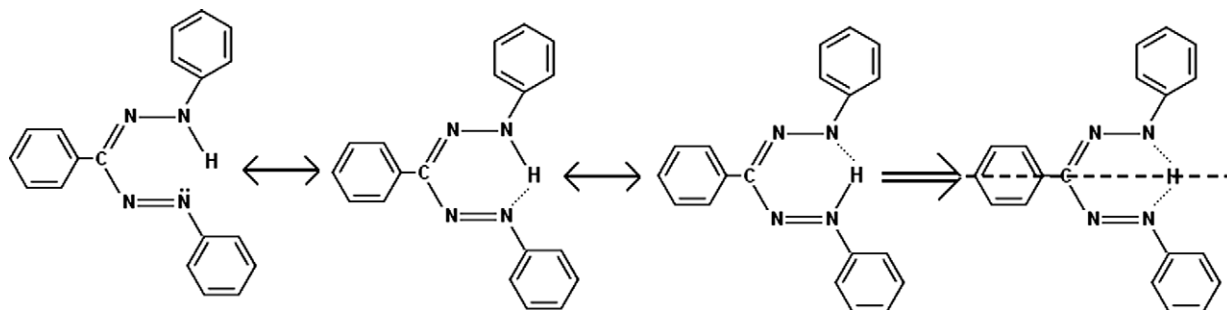


Scheme 2b. Possible oxidation mechanism for **3**, **6**.

TPF (**1**) is in chelate form with symmetry. The formation of a hydrogen bond between the electron pair on  $-\text{N}=\text{N}-$  and the hydrogen of  $\text{NH}$  turns the molecule into a chelate structure (Scheme 3) resulting in tautomerism [1–4].

When  $^{13}\text{C}$  NMR values of the substituted **2–7** are examined the *p*-substituted compounds give 15C signal due to chelation and symmetry mentioned above while *o*- and *m*-substituted compounds give 17C signal [1,3,12,13]. C peaks shift towards a lower field when the 1-phenyl ring includes Cl and Br substituents. For example, C=N imine carbon peaks in **2–7** appear at a lower field compared to unsubstituted parent TPF (**1**).

In the IR data of **1–7** given in Table 4 the C=N stretching band appears at  $1530\text{--}1520 \text{ cm}^{-1}$ . If the molecule has a chelate structure the C=N stretching band is observed at  $1500\text{--}1460 \text{ cm}^{-1}$  since the molecule is at a lower energy state due to the stability provided by  $\pi$ -electrons. When 1-phenyl and 3-phenyl rings are substituted with bulky groups these groups must push 5-phenyl rings. Therefore the chelate structure is distorted and a semi open or open structure is formed. At an open conformation the  $\pi$ -stability is distorted and the molecule is at a higher energy (excited) level. Therefore the C=N stretching band shifts to  $1560\text{--}1540 \text{ cm}^{-1}$  [3,12]. In this case, the semi open or open structures in this study must be

**Scheme 2c.** Possible oxidation mechanism of compounds 3 and 6.**Scheme 2d.** Possible oxidation mechanism of compounds 4 and 7.**Scheme 3.** Molecular chelation and symmetry.**Table 4**The IR spectral data of the formazans **1–7**, (in KBr,  $\text{cm}^{-1}$ )

Compound	Aromatic C–H	N–H	Aromatic C=C	C=N	–NO <sub>2</sub>	–Cl	–Br	N=N	CNNC structural vibration
<b>1</b>	3069	3050–3000	1600	1500	–	–	–	1450	930–905
<b>2</b>	3500–3410	3100–2900	1600	1530	1350	740	–	1250	820–650
<b>3</b>	3500–3400	3100–3080	1600	1530	1350	700	–	1250	820–680
<b>4</b>	3480–3400	3120–3080	1600	1535	1350	780	–	1250	890–680
<b>5</b>	3490–3410	3100–3070	1610	1520	1340	–	730	1250	810–650
<b>6</b>	3490–3410	2950–2850	1610	1520	1350	–	690	1220	800–650
<b>7</b>	3490–3410	2950–2850	1610	1540	1350	–	690	1220	800–650

at certain equilibrium since C=N stretching bands appear at 1530–1520  $\text{cm}^{-1}$  (Table 4).

Table 5 list all the peaks observed in the UV–vis spectra of the formazan and substituted **1–7**. Formazan  $\lambda_{\text{max}1}$  peaks are generally

observed at 410–500 nm and may shift to 550–600 nm depending upon the structure. These peaks are due to  $\pi$ – $\pi^*$  and  $n$ – $\pi^*$  electronic transitions in formazan skeleton (CNNC). The  $\lambda_{\text{max}2}$  peaks are sharp peaks which appear at 300–350 nm corresponds to

**Table 5**  
UV–visible absorption maxima of the formazans **1–7** (DMSO,  $10^{-5}$  mol/l)

Compound	$\lambda_{\max 1}/\text{nm}$ (Abs)	$\lambda_{\max 2}/\text{nm}$ (Abs)	Chemical shift, $\Delta\lambda_{\max}$
<b>1</b>	482.0 –(0.630)	380.0 –(0.232)	–
<b>2</b>	482.0 –(0.987)	405.0 –(0.264)	0
<b>3</b>	479.0 –(0.852)	395.0 –(0.179)	3
<b>4</b>	486.0 –(1.167)	399.0 –(0.212)	–4
<b>5</b>	483.0 –(0.318)	423.0 –(0.172)	–1
<b>6</b>	480.0 –(0.650)	406.0 –(0.263)	2
<b>7</b>	486.0 –(0.630)	405.0 –(0.223)	–4

Column 4:  $\Delta\lambda_{\max} = \lambda_{\max 1}$  (TPF) –  $\lambda_{\max 1}$  (substituted formazans).

electronic transitions  $\pi-\pi^*$  of  $-\text{N}=\text{N}-$  group in the molecule. Our discussion will focus on  $\lambda_{\max 1}$  values belonging to the broad

characteristic peaks of formazan skeleton. The chemical shift values ( $\Delta\lambda$ ) were determined by taking the difference between the  $\lambda_{\max 1}$  value of TPF (**1**) and  $\lambda_{\max 1}$  values of substituted formazans.

As seen from Table 5,  $\lambda_{\max 1}$  value of TPF (**1**) is observed at 482 nm. However  $\lambda_{\max 1}$  values for *o*-Cl and *o*-Br substituted (**2**, **5**) were observed at 482 nm and 483 nm, respectively. The Cl and Br inductive electron withdrawing and resonance electron donating effects impose an opposing effect on each other. Cl at the *o*-position must be balancing the electron withdrawing effect of  $\text{NO}_2$  group on the 3-phenyl ring due to its high electronegativity and elevated inductive effect at the *o*-position. The peaks obtained at the *m*- and *p*-positions are in accordance with the expectations. It is natural that Cl shifted  $\lambda_{\max 1}$  1 nm less than Br is due to the difference in their electronegativity values. At the *p*-position both

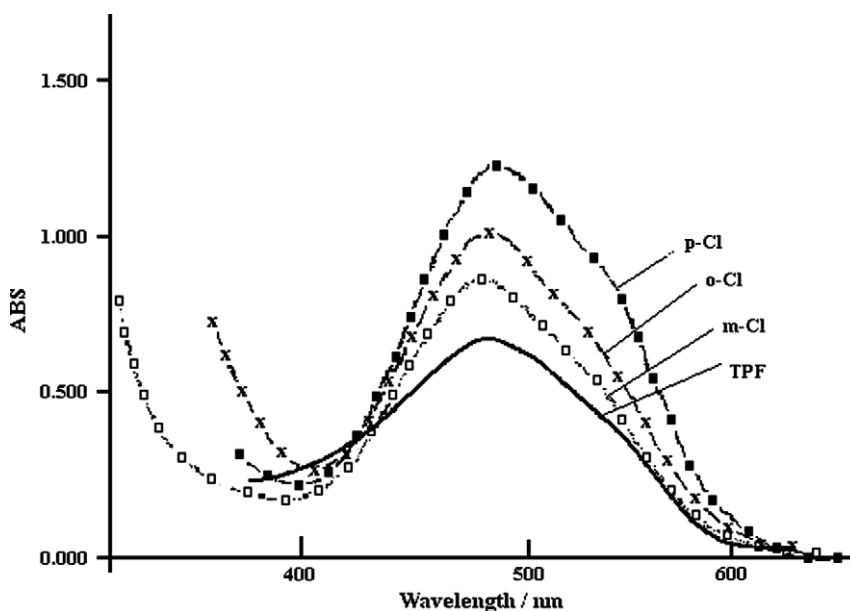


Fig. 6a. Absorption spectra of  $1.0 \times 10^{-5}$  M DMSO solutions of compounds **2–4** compared to TPF (**1**).

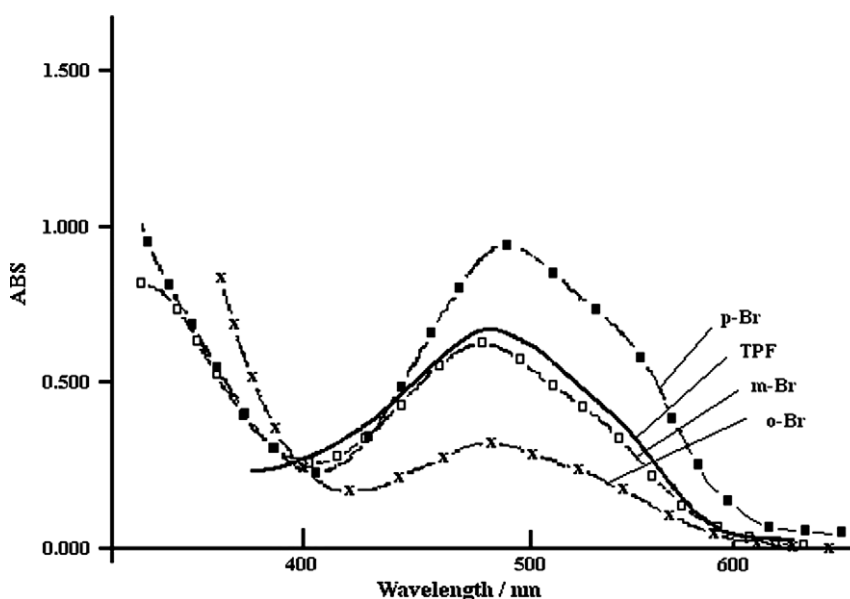


Fig. 6b. Absorption spectra of  $1.0 \times 10^{-5}$  M DMSO solutions of compounds **5–7** compared to TPF (**1**).

substituents shifted the  $\lambda_{\max 1}$  value to 486 nm and acted as electron donating groups due to resonance effect (5–7). Figs. 6a and 6b compare the  $\lambda_{\max}$  values of the *o*-, *m*-, *p*-positions of Cl and Br.

#### 4. Conclusions

Spectroscopic characteristics of the prepared complexes are discussed. Determined peak potentials ( $E_{\text{ox}}$ ,  $E_{\text{red}}$ ), diffusion coefficients, number of electrons transferred ( $n$ ) and heterogeneous rate constants ( $k_s$ ) were obtained with the use of cyclic voltammetry, linear sweep voltammetry and chronoamperometry. The oxidation products prepared by controlled potential electrolysis (CPE) were isolated and identified by different techniques: GC–mass and elemental analysis. The oxidation mechanism was occurred in a single-step two electron or two steps two electron transfer to forming tetrazolium salts. Additional support to the above proposed electro-oxidation scheme was found to be of importance. Thus, it appeared mandatory to study the effect of substituent on the reaction site of these compounds.

The spectral and redox properties were compared. There was a relatively correlation between the  $\lambda_{\max}$  and peak potentials ( $E_{\text{ox}1}$  and  $E_{\text{red}1}$  values) (Figs. 7 and 8). As seen from Table 1,  $E_{\text{ox}1}$  values observed at  $-1390.3$  mV in TPF (1) were shifted to  $-1171.7$  mV to  $-1289.4$  mV in the substituted formazans (2–7). The extent of this shift decreased in the order: *m*-Br > *p*-Br > *o*-Cl > *p*-Cl > *m*-Cl > *o*-Br, in accordance with the electron withdrawing (inductive effect) and donating (resonance effect) power of substituents.  $E_{\text{red}1}$  values observed at  $-426.0$  mV in TPF (1) were shifted to  $-552.1$  mV to  $-682.9$  mV in the substituted formazans (2–7). The extent of this shift decreased in the order: *p*-Cl > *p*-Br > *m*-Br > *o*-Br > *o*-Cl > *m*-Cl, in accordance with the electron withdrawing (inductive effect) and donating (resonance effect) power of substituents. The Cl and Br groups are electron withdrawing with regard to inductive effect but electron donating with regard to res-

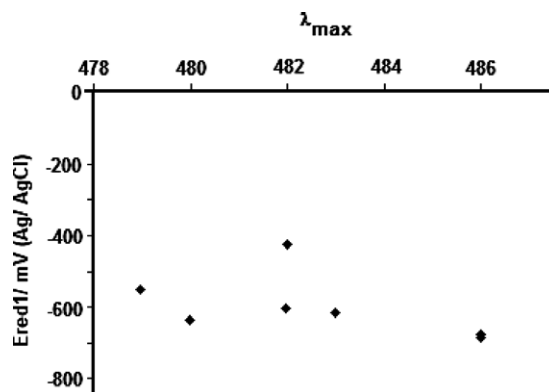


Fig. 8. The correlation between the  $\lambda_{\max}$  and the  $E_{\text{red}1}$ /mV (Ag/AgCl) values.

onance and their effect upon system is the summation of these two opposite effects. Their effects on the shift of  $E_{\text{ox}1}$  to the anodic region are large. The findings are as expected. But these results showed the effect of changing the type and the position of the substituent on the ring.

It was also investigated whether the Hammett substituent coefficients could be used to evaluate the total effect of the two different substituents, upon the  $\lambda_{\max}$  values and thus the color. The total  $\sigma_T$  ( $\sigma_1 + \sigma_2 = \sigma_T$ ) and related  $\lambda_{\max}$  values are at the Table 6. The total  $\sigma_T$  and related  $\lambda_{\max}$  values were plotted Fig. 9. As seen from Fig. 9, there is a linear relation between  $\sigma_T$  and  $\lambda_{\max}$  values. Therefore  $\sigma_T$  values can be used to evaluate the absorption  $\lambda_{\max}$  values and the effect of the substituents upon the rate of a oxidation process. Going from *p*-Br substituted formazan to *m*-Cl substituted formazan, the rate of oxidation process becomes higher. This result is in agreement with the fact that total  $\sigma_T$  values for *m*-Cl and *m*-Br substituted formazans are 1.08.

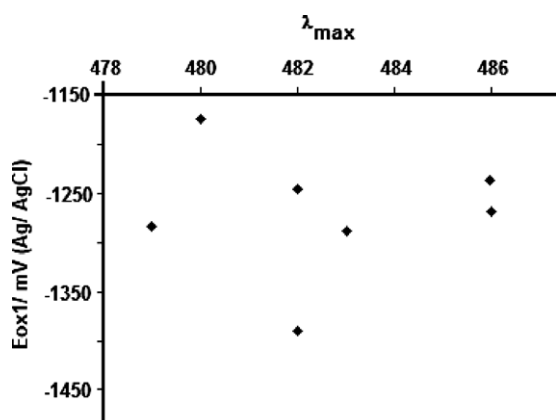


Fig. 7. The correlation between the  $\lambda_{\max}$  and the  $E_{\text{ox}1}$ /mV (Ag/AgCl) values.

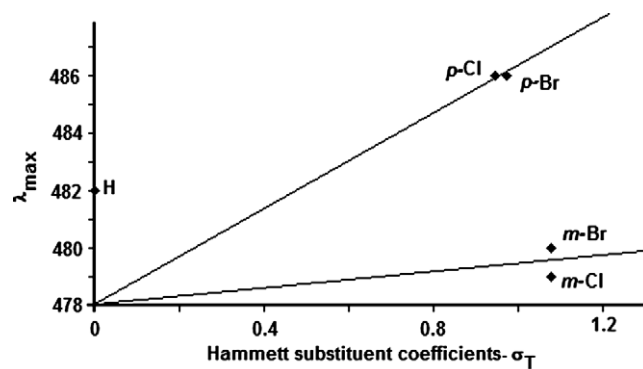


Fig. 9. The  $\lambda_{\max}$  values against the Hammett substituent coefficients- $\sigma_T$ .

Table 6

The total  $\sigma_T$  ( $\sigma_1 + \sigma_2$ ) and related  $\lambda_{\max}$  values

Substance position	Compound	Abbreviation	$\sigma'$ values	$\sigma_T$ (total effect)	$\lambda_{\max 1}$ /nm
<i>m</i> -	1	H	H: 0	0	482
	3	<i>m</i> -Cl, <i>m</i> -NO <sub>2</sub>	<i>m</i> -Cl: 0.37; <i>m</i> -NO <sub>2</sub> : 0.71	1.08	480
	6	<i>m</i> -Br, <i>m</i> -NO <sub>2</sub>	<i>m</i> -Br: 0.37; <i>m</i> -NO <sub>2</sub> : 0.71	1.08	479
<i>p</i> -	4	<i>p</i> -Cl, <i>m</i> -NO <sub>2</sub>	<i>p</i> -Cl: 0.24; <i>p</i> -NO <sub>2</sub> : 0.71	0.95	486
	7	<i>p</i> -Br, <i>m</i> -NO <sub>2</sub>	<i>p</i> -Br: 0.26; <i>p</i> -NO <sub>2</sub> : 0.71	0.97	486

## Acknowledgements

We are very grateful to the Gazi University Research Fund for providing financial support for this Project (No. 04/2004-13).

## References

- [1] U. Yüksel, Post Doctoral Thesis, Aegean University Turkish, 1981.
- [2] H. Tezcan, T. Uyar, Turkish J. Spect., Aegean University, 9 (1988) 8–19; H. Tezcan, T. Uyar, R. Tezcan, Turkish J. Spect., Aegean University, 10 (1989) 82–90.
- [3] H. Tezcan, N. Ozkan, Dyes Pigments 56 (2003) 159–166.
- [4] S. Erkoc, H. Tezcan, E.D. Calisir, F. Erkoc, Int. J. Pure Appl. Chem. 1 (1) (2006) 37–44.
- [5] V.C. Schiele, Ber. 30 (1964) 308–318.
- [6] A.M. Mattson, C.O. Jensen, R.A. Dutcher, Science 5 (1947) 294–295.
- [7] H. Wan, R. Williams, P. Doherty, D.F. Williams, J. Mater. Sci.: Mater. Med. 5 (1994) 154–159.
- [8] G.M. Abou Elenien, J. Electroanal. Chem. 375 (1994) 301–305.
- [9] T. Oritani, N. Fukuhara, T. Okajima, F. Kitamura, T. Ohsaka, Inorg. Chim. Acta 357 (2004) 436–442.
- [10] A.S. Baranski, W.R. Fawcett, C.M. Gilbert, Am. Chem. Soc. 57 (1) (1985) 166–170.
- [11] R.J. Klingler, J.K. Kochi, J. Phys. Chem. 85 (1981) 1731.
- [12] D.H. Williams, I. Fleming, Spectroscopic Methods In Organic Chemistry, McGraw-Hill Publishing Company Limited, London, 1966.
- [13] F. Schiman, Nuclear Magnetic Resonance Of Complex Molecules, vol. 1, Vieweg and Sohn GmbH, Braunschweig, 1970.